Linear and nonlinear physics of the magnetoacoustic cyclotron instability of fusion-born ions in relation to ion cyclotron emission

L. Carbajal,[1,a)] R. O. Dendy,[2,1] S. C. Chapman,[1,3,4] and J. W. S. Cook[1]
[1]*Centre for Fusion, Space and Astrophysics, Department of Physics, The University of Warwick, Coventry CV4 7AL, United Kingdom*
[2]*EURATOM/CCFE Fusion Association, Culham Science Centre, Abingdon OX14 3DB, Oxfordshire, United Kingdom*
[3]*Department of Mathematics and Statistics, University of Tromsø, N-9037, Tromsø, Norway*
[4]*Max Planck Institute for the Physics of Complex Systems, D-01187, Dresden, Germany*

(Received 18 November 2013; accepted 21 December 2013; published online 17 January 2014)

The magnetoacoustic cyclotron instability (MCI) probably underlies observations of ion cyclotron emission (ICE) from energetic ion populations in tokamak plasmas, including fusion-born alpha-particles in JET and TFTR [Dendy *et al.*, Nucl. Fusion **35**, 1733 (1995)]. ICE is a potential diagnostic for lost alpha-particles in ITER; furthermore, the MCI is representative of a class of collective instabilities, which may result in the partial channelling of the free energy of energetic ions into radiation, and away from collisional heating of the plasma. Deep understanding of the MCI is thus of substantial practical interest for fusion, and the hybrid approximation for the plasma, where ions are treated as particles and electrons as a neutralising massless fluid, offers an attractive way forward. The hybrid simulations presented here access MCI physics that arises on timescales longer than can be addressed by fully kinetic particle-in-cell simulations and by analytical linear theory, which the present simulations largely corroborate. Our results go further than previous studies by entering into the nonlinear stage of the MCI, which shows novel features. These include stronger drive at low cyclotron harmonics, the re-energisation of the alpha-particle population, self-modulation of the phase shift between the electrostatic and electromagnetic components, and coupling between low and high frequency modes of the excited electromagnetic field. © *2014 AIP Publishing LLC*. [http://dx.doi.org/10.1063/1.4861866]

I. INTRODUCTION

Energetic ions born in fusion reactions, notably the 3.5 MeV alpha-particles resulting from thermal deuterium-tritium (DT) fusion, will play a key role in future magnetically confined plasmas. These ions must provide most of the plasma heating required to achieve self-sustained nuclear burning. It is possible that the efficiency of this heating process may be reduced, to some extent, by the occurrence of velocity-space instabilities that take place on fast timescales, which are shorter than the timescale on which the fusion-born particles deliver their energy to the plasma through collisional processes.[1] An instability that is potentially in this category gives rise to the experimentally observed ion cyclotron emission (ICE). This phenomenon involves the emission, from spatially localised regions of tokamak plasmas, of intense suprathermal radiation which is spectrally peaked at sequential ion cyclotron harmonics. This radiation appears to result from a collective instability that is driven by a velocity distribution of energetic ions that approximates to a drifting ring-beam, which can arise naturally, through drift orbit excursions, in the outer midplane plasma. ICE was the first collective radiative instability driven by confined fusion-born ions that was observed in a tokamak plasma.[2,3] ICE was the only instability driven by confined fusion-born alpha-particles that was observed both in JET and TFTR from DT plasmas.[4–8] It was originally detected from injected beam ions[1,9,10] in tokamaks, and ICE in this category has been observed in the large tokamaks JT-60U (Ref. 11) and ASDEX-U (Ref. 12). In DIII-D, ICE has recently been used as a diagnostic[13] of energetic ions ejected from the core plasma by fishbone oscillations.

Understanding the physics of the ICE emission mechanism provides a specific observational test of the theory and interpretation of energetic particle effects in magnetic confinement fusion (MCF) plasmas in an operationally important parameter regime. Recent advances in computational power bring fresh insights into this topic. The analytical theory of ICE was originally developed in terms of the linear magnetoacoustic cyclotron instability (MCI).[14] This appears to capture many, but not all, of the key observed features of the ICE measurements in TFTR and JET experiments. In particular, the linear MCI gives rise to: simultaneous excitation of fast Alfvén waves at sequential multiple cyclotron harmonics of the alpha-particles[4] (cf. Fig. 1(a)); strong growth rates for waves propagating nearly perpendicular to the magnetic field; linear scaling of the growth rate with alpha-particle concentration; and doublet splitting of the spectral lines (cf. Fig. 11 of Ref. 6). Analytical treatments of the linear MCI in a context, which generalises the fast Alfvén wave to its two-dimensional equivalent in tokamak geometry, namely, the compressional Alfvén eigenmode, include those of Refs. 15 and 16. In the analytically tractable formulation of the linear MCI theory of Ref. 14, the local

a)Electronic mail: L.Carbajal-Gomez@warwick.ac.uk.

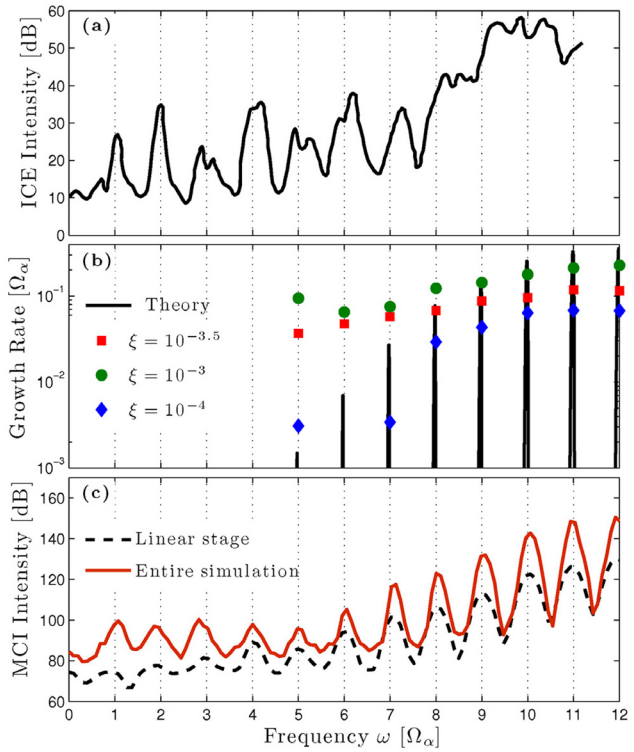

FIG. 1. Experimental, analytical, and numerical spectra. (a) Measured ICE intensity from JET PTE pulse 26 148. (b) Analytical linear growth rate for the MCI for the number density ratio, $\log_{10}(\xi) = -3$, along with the corresponding results from the hybrid simulations for the three values, $\log_{10}(\xi) = -4, -3.5, -3$. (c) Intensity of the electromagnetic field component B_z of the hybrid simulation with the parameters of the Sec. II A and number density ratio, $\xi = 10^{-3}$. The dashed black (solid red) line represents the linear (nonlinear) stage of the instability. Panel (a) reprinted with permission from Dendy *et al.*, Nucl. Fusion **35**(12), 1733 (1995). Copyright 1995 IOP Publishing.[6]

fusion-born alpha-particle population is modelled as a drifting ring-beam distribution in velocity space, with a delta function distributed perpendicular velocity, and a Maxwellian distribution of velocities parallel to the magnetic field, consistent with the alpha-particle birth energy 3.5 MeV. The success of linear theory, which by construction only addresses the early stage of growth, in explaining observed signal intensities, remained a paradox which has been partly resolved by the recent computational studies reported in Ref. 17. The results of the first fully self-consistent particle-in-cell (PIC) simulations of the MCI[17] validated the assumptions and predictions of linear theory, and showed good agreement with the properties of ICE measurements in JET. The work of Ref. 17 suggests that the congruence between linear theory and the observed signal intensities may reflect the prompt self-disruption, in velocity space, of the driving population by the waves which it excites. The full kinetics of both the electron population and the multiple ion populations was included in the PIC model of Ref. 17, and the inclusion of electron spatio-temporal scales imposed computational constraints on run time. In order to pursue MCI studies over longer timescales, we report here the results of numerical simulations of the MCI using a hybrid model for the plasma, where the ions are treated as particles and the electrons as a neutralizing, massless fluid. This model allows us to progress through the linear phase and far into the nonlinear phase of the MCI. It resolves features of the measured ICE signal that the linear theory was not able to capture, and also novel nonlinear processes. In the physics of the linear phase, we report, in particular, significantly improved agreement between simulated and observed ICE spectra at low cyclotron harmonics. In the physics of the nonlinear phase, we report, for example, re-energisation of the alpha-particles by transit time compressional magnetic pumping (TTCMP)[18,19] from waves excited earlier by the alpha-particles. This unexpected result reflects the fundamental theoretical plasma physics interest of the challenges posed by ICE. It is only now becoming possible to address the apparently simple question: if we create a minority drifting ring-beam population of energetic ions in a plasma, how do this population, the plasma, and the self-consistently excited wave fields evolve and interact over the long term?

II. THE HYBRID APPROXIMATION

We substantially extend the scope of the study of the MCI in Ref. 17 by performing simulations using the hybrid approximation. This enables us to address evolution over longer timescales than for the fully kinetic (PIC) simulations used in Ref. 17, at the price of not incorporating a full kinetic treatment of electron dynamics. This level of description is well adapted to phenomena occurring on lengthscales comparable to, or greater than, the ion inertial length, and on timescales comparable to the ion gyroperiod.[20,21] The hybrid model represents the different ion populations as particles and the electrons as a neutralizing, massless fluid. In this model the ion dynamics is governed by the Lorentz force

$$\frac{d\boldsymbol{x}_j}{dt} = \boldsymbol{v}_j\,, \tag{1}$$

$$m_j \frac{d\boldsymbol{v}_j}{dt} = eZ_j(\boldsymbol{E} + \boldsymbol{v}_j \times \boldsymbol{B})\,, \tag{2}$$

where $\boldsymbol{x}_j$ and $\boldsymbol{v}_j$ are the position and velocity of trajectories of ion of the species j, and m_j and Z_j are the corresponding mass and atomic number. On the other hand, the fluid electrons are modelled as an isotropic and isothermal ideal gas, $P_e = nT_e$. The electric ($\boldsymbol{E}(\boldsymbol{x},t)$) and magnetic ($\boldsymbol{B}(\boldsymbol{x},t)$) fields are linked by the generalized Ohm's law

$$\boldsymbol{E} = \frac{1}{\mu_0 en}(\nabla \times \boldsymbol{B}) \times \boldsymbol{B} - \boldsymbol{U}_i \times \boldsymbol{B} - \frac{1}{en}\nabla P_e\,, \tag{3}$$

and by Faraday's law

$$\frac{\partial \boldsymbol{B}}{\partial t} = -\nabla \times \boldsymbol{E}\,. \tag{4}$$

In deriving Eq. (3), we have substituted Ampere's law in its low-frequency limit (neglecting electron inertia and with length and timescales sufficiently large for quasineutrality to hold) into the electron momentum equation. This enables us to express the electric field in terms of ion variables in Eq. (3), notably, the ions' bulk velocity

$$\boldsymbol{U}_i = \frac{\sum_{j=1}^{N}(Z_j n_j \boldsymbol{u}_j)}{\sum_{j=1}^{N}(Z_j n_j)}. \quad (5)$$

Here, the summation is over N species of ions, $\boldsymbol{u}_j$ and n_j are the bulk velocity and ion number density of species j, whilst in Eq. (3) n refers to the total number density

$$n \equiv n_e = \sum_{j=1}^{N} Z_j n_j, \quad (6)$$

which is obtained from the quasineutrality condition. In our simulations, the fractional concentration of fusion-born alpha-particles with respect to deuterons, $\xi = n_\alpha/n_D$, is in the range of 10^{-3} to 10^{-4}. Equations (1)–(6) completely define the hybrid model for the multi-species case. The model allows the existence of low-frequency kinetic electrostatic modes such as ion-Bernstein waves, as well as electromagnetic modes including ion-cyclotron waves and Alfvén waves.

A. Hybrid simulations of the MCI

We have performed 1D3V numerical simulations (one-dimensional in position and three-dimensional in velocity space) of the MCI in the hybrid approximation, taking the direction of variation along the x-axis to be perpendicular to the constant background magnetic field $\boldsymbol{B}_0 = B_0\hat{z}$. Following Ref. 17, we initialise with an isotropic, thermal distribution of deuterons with initial temperature 1 keV, and a ring-like distribution of minority alpha-particles, $f_\alpha(v_\parallel, v_\perp) = \delta(v_\parallel)\delta(v_\perp - u_\perp)$ at 3.5 MeV. Here, $u_\perp$ is the magnitude of the initial perpendicular velocity of the alpha-particles, and the population is randomly uniformly distributed in initial gyro-angle. This distribution function corresponds to a simplified version of the one used in the analytical theory of the MCI in Ref. 7

$$f = \frac{1}{2\pi^{3/2} u_\perp v_r} \exp\left(-\frac{(v_\parallel - v_d)^2}{v_r^2}\right)\delta(v_\perp - u_\perp), \quad (7)$$

for the case where the parallel velocity, $v_\parallel$, and the average parallel drift speed, v_d, are zero. Here, v_r, is the parallel velocity spread of the energetic ions, which is also zero in our simulations.

In order to compare the results of our hybrid simulations with the ICE measurements, we set up values for the plasma parameters similar to those used in pulse 26 148 in the preliminary tritium experiment (PTE) in JET (cf. Table I of Ref. 4). The total number density in Eq. (6) and the electron temperature are set to $n = 10^{19}\,\mathrm{m}^{-3}$ and $T_e = 1\,\mathrm{keV}$, respectively. The strength of the background magnetic field corresponds to the value at the outer midplane in JET, $B_0 = 2.1\,\mathrm{T}$. The ratio of the minority alpha-particle number density to the deuteron number density, $\xi = n_\alpha/n_D$, which determines the growth rate of the excited waves in the linear theory of the MCI,[6] takes the value $\xi = 10^{-3}$ unless otherwise indicated. Our simulations do not take into account the collisional slowing-down of the alpha-particles, nor replenishment by freshly born particles. Thus, we focus exclusively on the fast timescale self-consistent physics of the MCI of a given energetic population, in both linear and nonlinear phases. As we shall see, our simulations reproduce the observed properties of ICE, suggesting that the relevant ion kinetic processes are captured in these simulations and in this simplified spatial topology with spatially homogeneous plasma.

To solve the pair of Eqs. (1) and (2), we employ a time-centered leap-frog scheme[22] and the spline-fitting weighting scheme to interpolate the fields from the grid and to extrapolate the density and currents to the grid.[23] Conversely, the electromagnetic fields of Eqs. (3) and (4) are solved using a periodic, staggered grid in space,[24,25] and a time-centered 4th-order Runge-Kutta scheme, together with a 4th-order Bashford-Adams extrapolation to calculate the current at the times where the electromagnetic fields are calculated.[26] Additionally, we introduce some numerical diffusion, which acts on the electromagnetic fields and ion bulk variables at each time step in order to stabilize the simulations.[27] In this way, we prevent the unbounded growth of short-wave noise in our simulations. The large simulation domain consists of 8192 equal grid cells, each of length equal to the deuteron gyro-radius $r_{L_D} = v_{T_D}/\Omega_D$, where v_{T_D} is the initial thermal velocity of the deuteron. This enables us to resolve in detail the alpha-particle gyrodynamics ($r_{L_\alpha}/r_{L_D} \approx 41$), while also providing adequate coverage of the deuteron gyromotion. We obtain high resolution in wavenumber space due to the large number of modes present in the simulation domain, which enables calculation of high resolution fast Fourier transforms.

In Fig. 1(c), we show the power spectra of the hybrid simulation for the linear (black trace) and nonlinear (red trace) stages. These are calculated by integrating the frequency-wavenumber space over the positive wavenumber domain $k > 0$. For the calculation of the linear (nonlinear) stage, we use simulation data from the time interval $t/\tau_\alpha = 1$ to $t/\tau_\alpha = 5$ ($t/\tau_\alpha = 1$ to $t/\tau_\alpha = 10$). Here, τ_α is the alpha particle gyroperiod. In the same figure are plotted for comparison: in panel (b), linear growth rates calculated from analytical theory, Eq. (8) of Ref. 7; and in panel (a), the ICE intensity of pulse 26 148 of the PTE in JET, which was measured using an ion cyclotron resonance heating (ICRH) antenna in receiver mode. The power spectrum of the simulation, and especially that encompassing the nonlinear phase of the MCI (red trace in Fig. 1(c)), recovers most of the observed features of the ICE signal Fig. 1(a). The intensity peaks appear at the same positions on the frequency axis, with the most intense peaks occurring for $\omega/\Omega_\alpha \geq 8$. The dashed black trace in Fig. 1(c) represents the power spectrum of the linear stage of the MCI simulation, already showing several key features of the ICE signal. In this respect, our hybrid simulation confirms previous analytical[5,7] and PIC computational[17] studies. In addition to the theoretically predicted growth rate (Eq. (8) of Ref. 7), Fig. 1(b) also shows the growth rate obtained from the early phase of hybrid simulations for three different values of ξ. We note

better agreement between these results for the harmonics $\omega/\Omega_\alpha \geq 7$ than for the lower excited harmonics in our simulations, down to $\omega = 5\Omega_\alpha$. Also, as predicted by the linear theory, the growth rates increase with the concentration of alpha-particles. The parameters used in the calculation of the analytical linear growth rate[7] are: an angle of propagation $\theta = 88°$, and a narrow spread of the parallel velocity of the minority alpha-particles, $v_r/u_\perp \approx 0.06$, which approximate the set-up of our simulations. Further hybrid simulations of the MCI for different propagation angles, $85° \leq \theta \leq 90°$, follow the predictions of the linear theory for the growth rates,[7] decreasing as the propagation angle decreases whilst keeping constant the concentration of alpha-particles ξ.

Importantly, the fact that the hybrid model enables us to follow the MCI deep into its nonlinear phase enables this treatment to capture additional aspects of the observed ICE signal. Comparison of the two traces for the simulated MCI in Fig. 1(c) with the measured ICE signal in Fig. 1(a) shows that only the solid red trace, which encompass the nonlinear phase, robustly captures the lower observed cyclotron harmonic peaks one to three, which appear to become unstable due to nonlinear interactions between modes excited in earlier times, as explained in Sec. II B.

As we mentioned before, plasma heating by fusion-born ions requires the energetic alpha-particles to transfer their energy to the background electrons and ions. In Fig. 2, we show the time evolution of the change in particle energy density and the energy density of the excited electric and magnetic fields associated with the MCI. At $t/\tau_\alpha = 1$, the instability starts to take over. The free energy of the alpha-particles contributes to energising the background deuterons which oscillate in the electrostatic ($E_x(x,t)$) and electromagnetic fields ($B_z(x,t)$) excited by wave-particle cyclotron resonance of the alpha-particles. This process, the energy transfer to the deuterons, peaks at $t/\tau_\alpha \approx 5$, giving way to the re-energisation of the alpha-particles, which is discussed in Sec. II C.

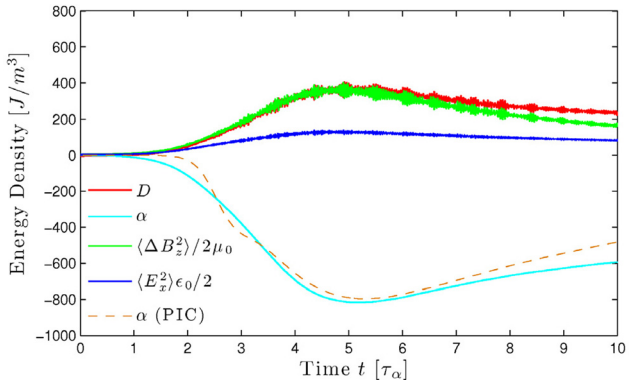

FIG. 2. Time evolution of the change in particle energy density of the field components. The traces are, ordered from the top downwards (and in colour online) at $t = 10\tau_\alpha$: Top (red) the change in the kinetic energy density of deuterons; second (green) the energy density of the magnetic field perturbation, $\Delta B_z \equiv B_z(x,t) - B_0$, third (blue) the energy density of the electrostatic field E_x; fourth (orange dashed) the change in kinetic energy density of the alpha-particles taken from a PIC simulation with the same parameters as our hybrid simulation; bottom (cyan) the change in kinetic energy density of the alpha-particles of our hybrid simulation. The time axis of the trace corresponding the PIC simulation has been divided by a factor of two given that it takes longer for the instability to develop in this case.

B. Electric and magnetic fields

We now turn to the time evolution of the electric and magnetic fields. Panels (a) and (d) of Fig. 3 plot $\log_{10}$ of the spectral density of the oscillatory part of B_z in frequency-wavenumber space for the linear and nonlinear stages. The dashed lines in these panels show $\omega/k = V_A$, the dispersion relation of the fast Alfvén wave. We see that modes of the fast Alfvén wave are excited in the simulations at resonances with consecutive ion cyclotron harmonics of the alpha-particles. Panels (b) and (e) of Fig. 3 show a close-up of the most strongly excited modes for the linear and nonlinear stages, respectively. Here, the intersection of the vertical and horizontal dashed lines indicates the maximum of the spectral density at $\omega/\Omega_\alpha \approx 11$ and $kV_A/\Omega_\alpha \approx 11.5$. Panels (c) and (f) show the time evolution in wavenumber space of the B_z field component. This shows that the most strongly excited modes are in the range $6 \leq kV_A/\Omega_\alpha \leq 13$, so that the characteristic length scales of these modes correspond to the initial gyroradius of the alpha-particles, $r_{L\alpha} = u_\perp/\Omega_\alpha$.

Figure 4 shows the contribution of each positive wavenumber ($k > 0$) to the energy density of the fields. Panels (a) and (b) of Fig. 4 plot this for the linear and nonlinear stages, respectively. For the calculation of the linear (nonlinear) stage we used simulation data from the time interval $t/\tau_\alpha = 1$ to $t/\tau_\alpha = 5$ ($t/\tau_\alpha = 1$ to $t/\tau_\alpha = 10$). We see spectra with consecutive intensity peaks in the range $6 \leq kV_A/\Omega_\alpha \leq 13$, for all the non-zero field components. By comparing with panels (e) and (f) of Fig. 3, these intensity peaks can be identified with the resonances of the fast Alfvén wave at consecutive ion cyclotron harmonics of the alpha-particles. It is evident from Fig. 4 that the electromagnetic component B_z contains more energy for the wavenumbers $kV_A/\Omega_\alpha < 13$ than the electrostatic component E_x. The main difference between the linear and nonlinear stages is the higher energy of the electromagnetic component B_z in the range $kV_A/\Omega_\alpha < 5$ (cf. Fig. 4(b)), which is not predicted by the linear theory of the MCI.

Let us now consider the interaction between the electric and magnetic fields that is mediated by the plasma. First, we calculate the spatial cross-correlation, over an arbitrary separation Δx, between the normalised components $B_z(x,t)/\sqrt{2\mu_0}$ and $\sqrt{\epsilon_0/2}E_x(x,t)$

$$R(\Delta x, t) = \frac{1}{2}\sqrt{\frac{\epsilon_0}{\mu_0}}\int B_z(x+\Delta x, t)E_x(x,t)dx, \qquad (8)$$

where the integral is performed over the entire simulation domain. To construct the most appropriate corresponding phase shift, we calculate the phase shift between the field components

$$\Delta\phi = k^*\Delta x, \qquad (9)$$

where $k^*V_A/\Omega_\alpha \approx 11.5$ is the dominant wavenumber in our simulation. This enables us to transform from $R(\Delta x, t)$ to $R(\Delta\phi, t)$, which is plotted in Fig. 5. This shows that in the early stages of our simulation there is not a well defined phase shift between the electric and magnetic fields. However, as the simulation enters the nonlinear stage, the coupling between the fields produces a phase shift $\Delta\phi \approx \pi$ for $t > 5\tau_\alpha$.

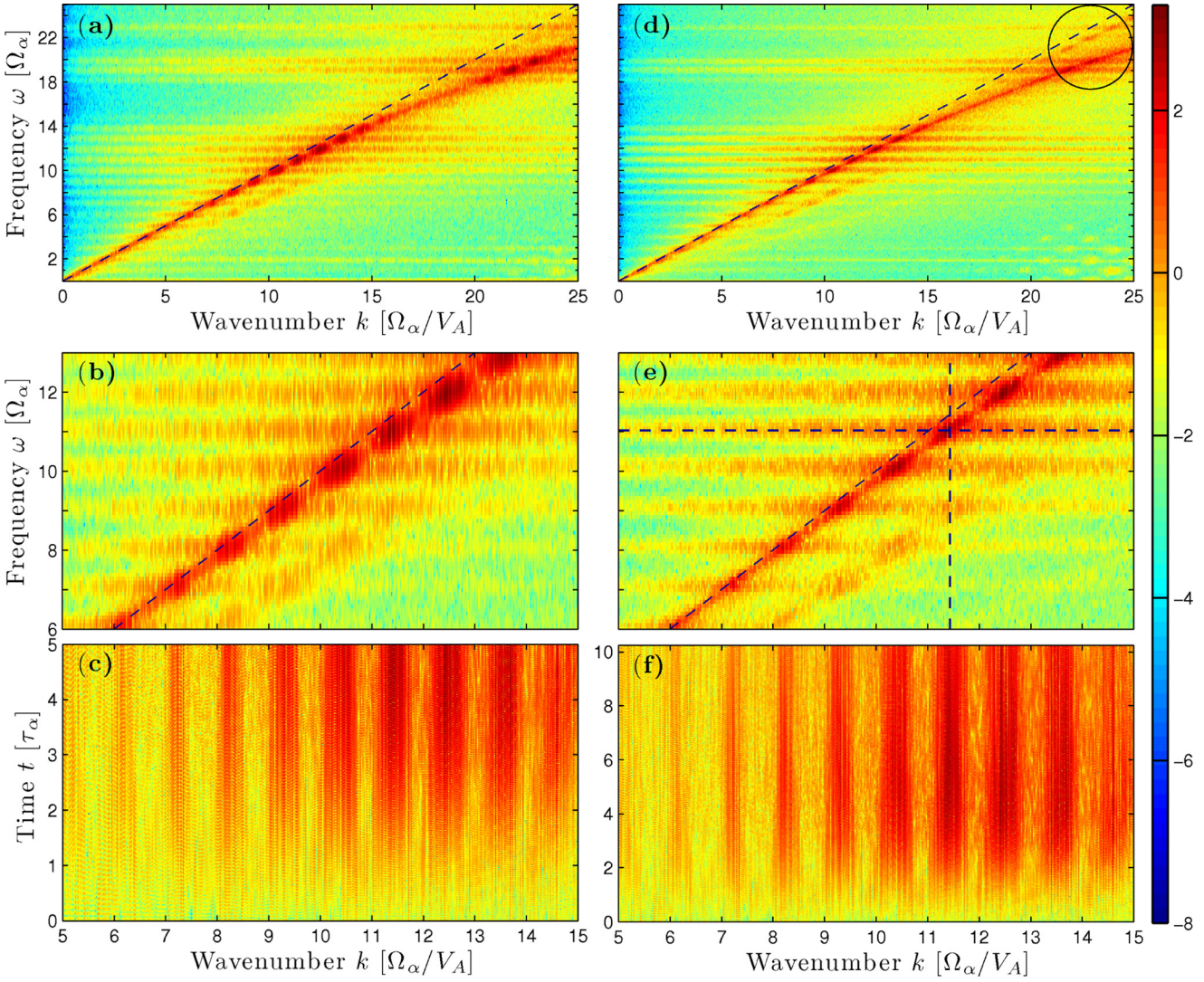

FIG. 3. Frequency and wavenumber space for the linear (panels (a)–(c)) and nonlinear stages (panels (d)–(f)) of the MCI. Panels (a) and (d): shading indicates the $\log_{10}$ of the spectral density of the oscillatory part of the B_z field component in frequency-wavenumber space. These plots show the excitation of the fast Alfvén wave with resonances at consecutive ion cyclotron harmonics, $\omega = n\Omega_\alpha$, where n is a positive integer. The dashed line shows, $\omega/k = V_A$, where $V_A = B_0/\sqrt{\mu_0 n_i m_D}$ is the Alfvén velocity. The ellipse in (d) shows the excited modes due to the alpha-particles' re-energisation. Panels (b) and (e): close-up of the most strongly excited modes in frequency-wavenumber space. The intersection of the vertical and horizontal dashed lines in panel (e) points to the maximum of B_z^2 in frequency-wavenumber space at $\omega/\Omega_\alpha \approx 11$ and $kV_A/\Omega_\alpha \approx 11.5$. Panels (c) and (f): time evolution of the wavenumber spectra of the field component B_z.

Let us now examine whether there is nonlinear coupling between the well-defined approximate normal modes at successive ion cyclotron harmonics that are found in the present simulation. It is of particular interest, and exploits the hybrid simulation approach, to compare any such coupling in the early and later stages of the MCI. An appropriate technique is bispectral analysis,[28,29] which has been successfully applied to experimental measurements on magnetically confined plasmas, for example, Refs. 30 and 31. For present purposes, this requires calculation of the non-normalised self-bicoherence of the oscillatory part of B_z in wavenumber space

$$b^2(k_1, k_2) = |\langle \hat{B}_z^*(k_1 + k_2)\hat{B}_z(k_1)\hat{B}_z(k_2)\rangle|^2, \qquad (10)$$

where $\hat{B}_z(k)$ is the Fourier transform of $B_z(x)$ and $\hat{B}_z^*(k)$ its complex conjugate. Here, the average $\langle\cdot\rangle$ is taken over a small time window of width $\Delta t \sim 0.2\tau_\alpha$. We show this calculation in Fig. 6, where the shading indicates the intensity of coupling between different modes. The red colour indicates significant coupling between two different modes. We see strong coupling in the linear (Fig. 6(a)) and nonlinear (Fig. 6(b)) stages between pairs of modes (k_1, k_2) that both have $kV_A/\Omega_\alpha \approx 10$, with less intense coupling for pairs in the linear stage that have $k_1 V_A/\Omega_\alpha \approx 10$ and $k_2 V_A/\Omega_\alpha \approx 1$. However, in the nonlinear stage (cf. Fig. 6(b)), all these points become equally intense, reflecting a more intense coupling between the relevant modes. These results may be extrapolated to the frequency domain by using the dispersion relation of panels (a) and (d) of Fig. 3. This indicates that the excitation of unstable modes at $\omega/\Omega_\alpha = 1, 2$, and 3 in the nonlinear stage (cf. Fig. 1(c)) is a result of the wave-wave coupling with the unstable modes in the range $8 \leq \omega/\Omega_\alpha \leq 12$.

C. Nonlinear stage of the MCI

Thus far, we have focused primarily on establishing congruence between our hybrid simulations of the MCI and

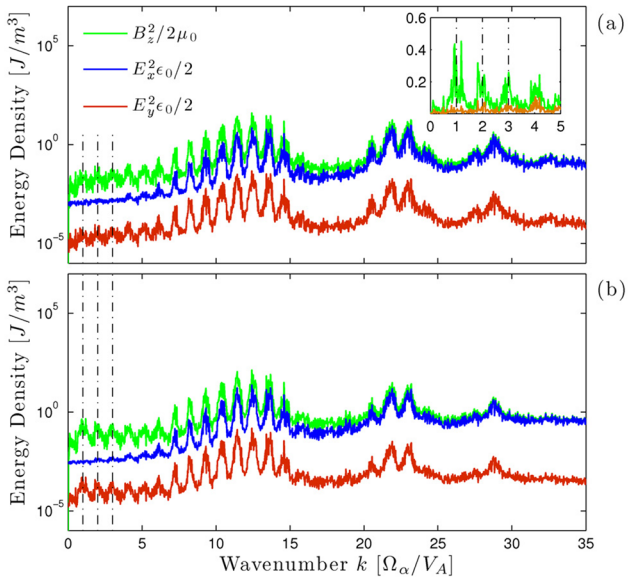

FIG. 4. Energy density of each non-zero field component as a function of positive wavenumber ($k>0$) in the linear (a) and nonlinear (b) stages. Strong localized peaks in the range $6 \leq kV_A/\Omega_\alpha \leq 13$ correspond to the resonances of the fast Alfvén wave at consecutive ion cyclotron harmonics of the alpha-particles. The intensity peaks about $kV_A/\Omega_\alpha = 22$ are important in the re-energisation process for alpha-particles in the nonlinear stage (cf. Figs. 2 and 3(d)). The vertical dotted-dashed lines show the position of the modes at $kV_A/\Omega_\alpha \approx 1, 2$ and 3, which are exited in the nonlinear stage. The inset panel in (a) plots the electromagnetic field energy density of B_z, on a linear scale, in the low cyclotron harmonic frequency region, for the nonlinear (green trace) and linear (orange) phases.

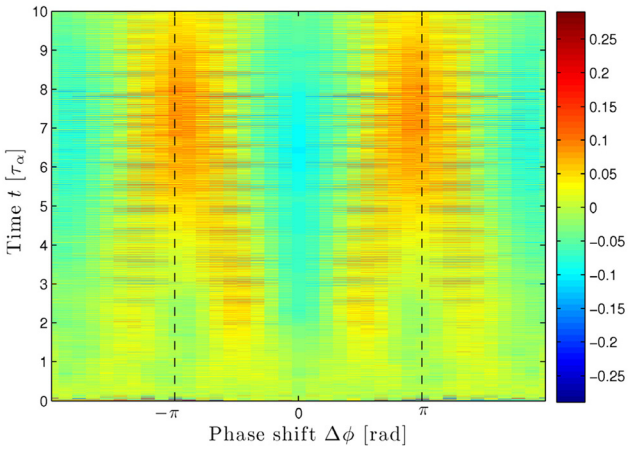

FIG. 5. Spatial cross-correlation $R(\Delta\phi, t)$ (cf. Eqs. (8) and (9)) between the normalised field components $B_z(x,t)/\sqrt{2\mu_0}$ and $\sqrt{\epsilon_0/2}E_x(x,t)$. The red (blue) colour indicates maxima (minima) of $R(\Delta\phi, t)$, indicating strong (lack of) correlation for the relative phase shift $\Delta\phi$. The vertical dashed lines show π and $-\pi$. The nonlinear interaction between the electric and magnetic fields produces a phase shift that remains almost constant at $\Delta\phi \approx \pi$ for $t > 5\tau_\alpha$.

three strands of previous research: observations of ICE,[1–4] linear analysis of the MCI,[6–9] and large scale numerical simulations of the MCI[17] using a PIC code which captures the full kinetics of ions and (unlike the hybrid model) electrons. We now turn to the key aspect of nonlinear phenomenology of the MCI, adumbrated in the preceding discussion of results, which can only be captured by a hybrid model given computational resource constraints. We focus first on the re-energisation of the alpha-particles visible in Fig. 2, commencing at $t/\tau_\alpha \approx 5$. In the time interval, $5 < t/\tau_\alpha < 7$, the energy of the background deuterons and the fields decreases gradually whilst the kinetic energy of the alpha-particle population reverses its previous decline. After this time, the background deuterons' energy remains approximately constant while the energy of the fields continues to decrease, being transferred to the alpha-particles as kinetic energy.

As a first step towards understanding this re-energisation process, we look at the velocity-position phase space of the alpha-particles, together with their velocity probability density function. In the right panel of Fig. 7, we show the smoothed, filled contours of the phase space of the alpha-particles at $t/\tau_\alpha \approx 9$, calculated by averaging over 16 windows of the phase space along the x-axis. The different colours here represent the value of $f_\alpha(x,v)$, where $v = \sqrt{v_x^2 + v_y^2}$ is the amplitude of the velocity of the alpha-particles. Here, we do not include the parallel velocity v_z, which remains constant in time for the chosen initial condition. We compare $f_\alpha(x,v)$ with the left panel of Fig. 7, which shows $f_\alpha(v)$ at three different times. In the linear stage, $f_\alpha(v)$ seems to follow a biased diffusive process in velocity space, leading up to the early time at $t/\tau_\alpha \approx 5$. Then, as the

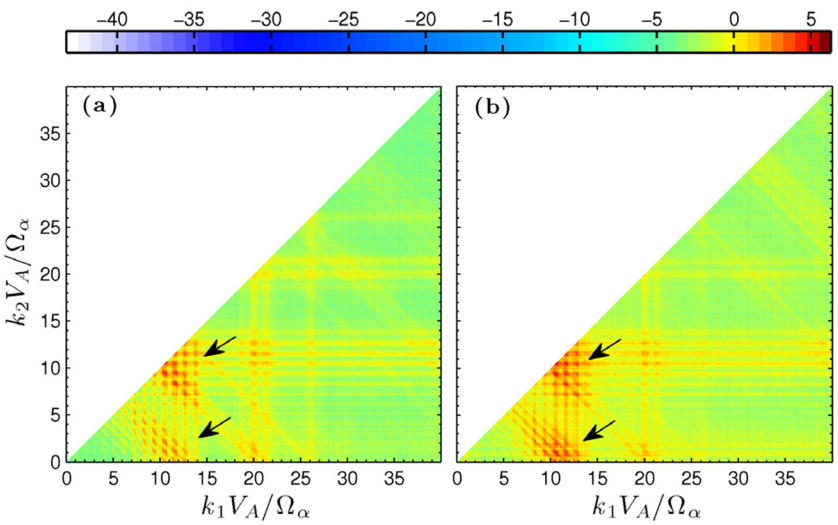

FIG. 6. Non-normalized self-bicoherence of the B_z component in wavenumber space, plotted using a $\log_{10}$ colour scale. Only the principal domain of the self-bicoherence is shown. The red colour indicates significant coupling between different modes at k_1 and k_2. Panels (a) and (b) show the non-normalised self-bicoherence of B_z in the linear stage at $t = 4\tau_\alpha$ and in the nonlinear stage at $t = 8\tau_\alpha$. The arrows in both panels point to areas on the k_1, k_2 plane, which show strong coupling between different modes.

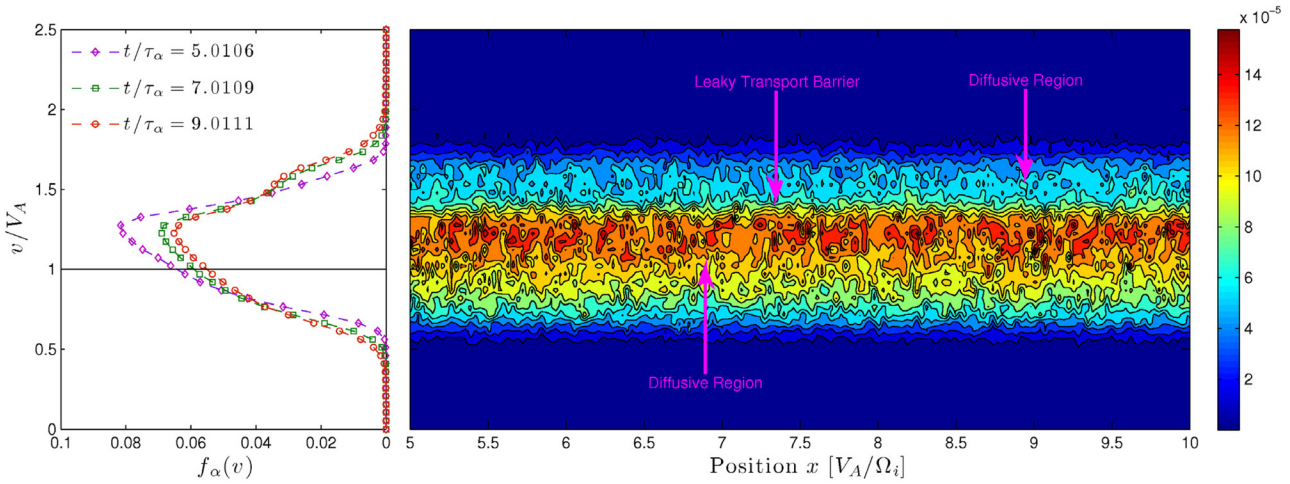

FIG. 7. Re-energisation of the alpha-particle population during the nonlinear phase of the MCI. Left panel: probability density function of the minority alphas, $f_\alpha(v)$, as a function of the magnitude of their velocity $v = \sqrt{v_x^2 + v_y^2}$, at three different times in the nonlinear stage of the hybrid simulation. The energisation of the alpha-particles is seen as the bump in $f_\alpha(v)$, which builds up in the nonlinear stage around $v/V_A \approx 1.5$. At this stage, the particles reach velocities higher than the birth velocity $u_\perp/V_A \approx 1.2$. Right panel: filled contours represent the smoothed probability density function $f_\alpha(x, v)$ of the minority alpha-particles as a function of position and velocity at $t/\tau_\alpha \approx 9$. The temporal evolution of $f_\alpha(v)$ and $f_\alpha(x, v)$ suggests the existence of two phase space diffusive regions, where the smaller diffusion region can be identified with the bump of $f_\alpha(v)$ in the left panel, and a leaky transport barrier, which produces the steep slope before the bump in $f_\alpha(v)$.

instability enters the nonlinear stage, a bump in $f_\alpha(v)$ starts to build up around $v/V_A \approx 1.5$. Once this bump of re-energised alpha-particles forms, we can identify three corresponding features in the phase space of Fig. 7, right panel: two phase space diffusion regions around $v/V_A \approx 1$ and $v/V_A \approx 1.5$ separated by a zone, which acts as a leaky transport barrier, which produces the steep slope before the bump in $f_\alpha(v)$.

It appears possible to identify the specific plasma physics mechanism that drives this re-energisation process. Using the data from Fig. 2, we calculate the fast Fourier transform of the change in the kinetic energy density of the alpha-particle population and the electromagnetic energy density associated with field component B_z. This calculation reveals three intense peaks at the frequencies $\omega/\Omega_\alpha = 20, 22,$ and 24, of which the peak at $\omega/\Omega_\alpha = 22$ is the most intense by far. These frequencies correspond to the modes highlighted in Fig. 3(d) and to the peaks in Fig. 4 around $kV_A/\Omega_\alpha = 22$. These modes have a phase velocity close to the Alfvén speed, which suggests that the mechanism driving the re-energisation of the alpha-particles is related to the fast Alfvén wave. The leading candidate mechanism is TTCMP.[18,19] This arises from the phase delay between the oscillations of the magnetic field and the induced oscillations in the perpendicular pressure of the alpha-particle population.[19] The TTCMP heating rate is given by[18]

$$\frac{dT_\alpha}{dt'} \sim 2\pi \frac{\omega}{\Omega_\alpha} T_\alpha \left(\frac{\tilde{B}}{B_0}\right)^2, \tag{11}$$

where T_α and $\tilde{B}$ are, respectively, the alpha-particle temperature and the amplitude of the oscillatory part of the magnetic field, and ω is the dominant frequency of wave oscillation. Here, $t' = t/\tau_\alpha$ is the dimensionless time used in the simulations. Figure 8 shows (top) $\mathrm{d}T_\alpha/\mathrm{d}t'$ inferred from the evolving alpha-particle population in our hybrid simulation using $T_\alpha \sim \langle m_\alpha v^2/2 \rangle$, together with (bottom) the analytical result Eq. (11) calculated from the numerical values of simulation variables. For this calculation, we used $\tilde{B}/B_0 \sim 0.01$ and $\omega/\Omega_\alpha = 22$. We observe that the heating rate predicted by Eq. (11) (solid black line) lies within 14% (blue dashed lines) of the heating rate observed in the simulation (solid red line).

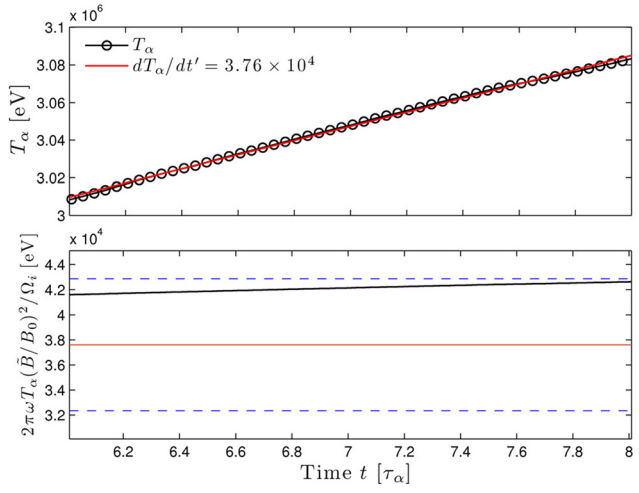

FIG. 8. Time evolution of alpha-particle temperature $T_\alpha \sim \langle m_\alpha v^2/2 \rangle$ during the nonlinear stage of the MCI from $t/\tau_\alpha = 6$ to 8. Top panel: T_α inferred from the kinetic alpha-particles in the simulation, together with best linear fit to $\mathrm{d}T_\alpha/\mathrm{d}t'$. Bottom panel: value of $\mathrm{d}T_\alpha/\mathrm{d}t'$ calculated using Eq. (11) for the numerical values of variables in the simulation, with $\omega/\Omega_\alpha = 22$. The heating rate predicted by the TTMCP theory (solid black line) lies within 14% (blue dashed lines) of the heating rate observed in the simulation (solid red line).

III. CONCLUSIONS

Hybrid simulations of the MCI, presented here, deepen understanding of the links between the physics of this instability and the observational features of ICE from energetic

ion populations in tokamak plasmas. Some—indeed many—of these features are known from the analytical linear theory of the MCI[5,7] and from recent fully kinetic PIC simulations.[17] The hybrid approximation, which incorporates fluid rather than kinetic electrons, has enabled us here to pursue simulations longer in time, and deep into the nonlinear phase of the MCI. We have focused on comparison with the measured ICE signal from the Preliminary Tritium Experiment in JET,[4,8] which has long been interpreted in terms of the MCI.[7,14,17] In this context, a number of novel phenomena emerge from the present work.

First, by extending into the nonlinear phase of the MCI, we recover substantial emission at the lowest spectral peaks, lying at the cyclotron harmonics one to three. These are present in the observed ICE signal, but calculations suggest they may well be linearly stable. They are not well resolved, if present at all, in PIC simulations that extend over shorter time duration than the present hybrid results. It appears that these lowest spectral peaks arise from nonlinear physics which is captured here for the first time. Specifically, the amplitude of these modes is larger due to wave-wave interaction between higher harmonics localized around $kV_A/\Omega_\alpha \sim 11$ (cf. Fig. 6(b)). This is also evident from Fig. 4, where a gain of energy density at small wavenumbers is visible in panel (b).

Second, we have identified the novel and unexpected feature of re-energisation of the alpha-particle minority at later times, as a consequence of wave-particle resonance with waves spontaneously excited by the alpha-particle population at earlier times. Analysis of our simulation results shows that the plasma physics process responsible is transit time compressional magnetic pumping (TTCMP). The excitation of the electromagnetic component B_z of the fast Alfvén wave in the linear stage, which drives the re-energisation of the alpha-particles in the nonlinear stage by TTCMP, is visible for the first time in the present simulations. A further related novel consequence is the excitation of second harmonics of the fast Alfvén wave ($\omega/\Omega_\alpha \sim 22$) due to the wave-particle interaction between the re-energised alpha-particles and the fast Alfvén wave.

The results presented here link well to prior work that used other approaches and necessarily focused on earlier phases of the MCI, and broadly validate it. We see the excitation of fast Alfvén waves at consecutive ion cyclotron harmonics of the alpha-particles in the range $5 < \omega/\Omega_\alpha < 12$, which play a key role in the linear stage transferring energy from the alpha-particles to the background deuterons. We have checked the predictions of analytical theory for the magnitude of the growth rates of the unstable modes, as well as their localization in the frequency domain and the magnitudes of their vector field components. Here too, the hybrid approach enables further insights into the physics. For example, we studied the plasma-mediated interaction between the electromagnetic component B_z and the electrostatic component E_x, which are excited in the linear stage of the MCI. As the simulation enters the nonlinear stage, we observe the self-modulation of the phase shift between the electrostatic (E_x) and the electromagnetic (B_z) fields, see for example Fig. 5.

We infer that it is very probable that the plasma physics process underlying ICE is the MCI. This was strongly suggested by the original analysis of JET and TFTR D-T plasma observations of ICE, in terms of the linear analytical theory of the MCI, and appears to be confirmed by the first principles large scale numerical simulations using PIC[17] and, here, hybrid codes. This depth of understanding of the emission mechanism is essential if ICE is to be exploited as a diagnostic of confined and lost fusion alpha-particles in ITER, as has been proposed. We note two further steps that could usefully be taken in the modelling of the MCI for ICE applications. First, there is the extension of the present 1D3V approach to the more computationally intensive 3D3V, so as to incorporate realistic tokamak spatial and magnetic field geometry, and thus simulate chunks of tokamak plasma. Second, there is the need to replenish the alpha-particle population through continuing birth in fusion reactions, and to slow and disperse it through collisions. We remark that the success of simulations that neglect this second aspect, in terms of replicating observational features of ICE, presumably reflects a separation of timescales. Our simulations indicate that most of the key physics unfolds on the rapid timescale of a few cyclotron periods, which is short compared to the evolution timescale of the overall alpha-particle population in quasi-steady state. Finally, the fundamental plasma physics question posed towards the end of the Introduction appears closer to being answered.

ACKNOWLEDGMENTS

L.C. acknowledges the Mexican Council of Science and Technology (CONACyT) for support. This work was part-funded by the EPSRC and the RCUK Energy Programme under Grant No. EP/I501045 and the European Communities under the contract of Association between EURATOM and CCFE. The views and opinions expressed herein do not necessarily reflect those of the European Commission. We also thank the EPOCH development team for their work on the PIC code adapted for this research. To obtain further information on the data and models underlying this paper please contact PublicationsManager@ccfe.ac.uk.

[1]W. Heidbrink and G. Sadler, Nucl. Fusion **34**, 535 (1994).
[2]G. A. Cottrell and R. O. Dendy, Phys. Rev. Lett. **60**, 33 (1988).
[3]P. Schild, G. Cottrell, and R. Dendy, Nucl. Fusion **29**, 834 (1989).
[4]G. Cottrell, V. Bhatnagar, O. D. Costa, R. Dendy, J. Jacquinot, K. McClements, D. McCune, M. Nave, P. Smeulders, and D. Start, Nucl. Fusion **33**, 1365 (1993).
[5]S. Cauffman, R. Majeski, K. McClements, and R. Dendy, Nucl. Fusion **35**, 1597 (1995).
[6]R. Dendy, K. McClements, C. Lashmore-Davies, G. Cottrell, R. Majeski, and S. Cauffman, Nucl. Fusion **35**, 1733 (1995).
[7]K. G. McClements, R. O. Dendy, C. N. Lashmore-Davies, G. A. Cottrell, S. Cauffman, and R. Majeski, Phys. Plasmas **3**, 543 (1996).
[8]K. G. McClements, C. Hunt, R. O. Dendy, and G. A. Cottrell, Phys. Rev. Lett. **82**, 2099 (1999).
[9]R. O. Dendy, K. G. McClements, C. N. Lashmore-Davies, R. Majeski, and S. Cauffman, Phys. Plasmas **1**, 3407 (1994).
[10]G. A. Cottrell, Phys. Rev. Lett. **84**, 2397 (2000).
[11]M. Ichimura, H. Higaki, S. Kakimoto, Y. Yamaguchi, K. Nemoto, M. Katano, M. Ishikawa, S. Moriyama, and T. Suzuki, Nucl. Fusion **48**, 035012 (2008).
[12]R. D'Inca, M. Garcia-Munoz, G. Tardini, and J.-M. Noterdaeme, in *Proceedings of the 38th EPS Conference on Plasma Physics* (Curran Associates, Inc., Strasbourg, France, 2012), P. 1.053.

[13]W. W. Heidbrink, M. E. Austin, R. K. Fisher, M. Garca-Muoz, G. Matsunaga, G. R. McKee, R. A. Moyer, C. M. Muscatello, M. Okabayashi, D. C. Pace, K. Shinohara, W. M. Solomon, E. J. Strait, M. A. V. Zeeland, and Y. B. Zhu, Plasma Phys. Controlled Fusion **53**, 085028 (2011).
[14]R. O. Dendy, C. N. Lashmore-Davies, K. G. McClements, and G. A. Cottrell, Phys. Plasmas **1**, 1918 (1994).
[15]N. Gorelenkov and C. Cheng, Nucl. Fusion **35**, 1743 (1995).
[16]H. Smith, T. Fülöp, M. Lisak, and D. Anderson, Phys. Plasmas **10**, 1437 (2003).
[17]J. W. S. Cook, R. O. Dendy, and S. C. Chapman, Plasma Phys. Controlled Fusion **55**, 065003 (2013).
[18]J. Vaclavik and K. Appert, Nucl. Fusion **31**, 1945 (1991).
[19]M. Brambilla, Plasma Phys. **16**, 482 (1974).
[20]D. Winske and N. Omidi, J. Geophys. Res.: Space Phys. **101**, 17287 (1996).
[21]S. E. Clark, D. Winske, D. B. Schaeffer, E. T. Everson, A. S. Bondarenko, C. G. Constantin, and C. Niemann, Phys. Plasmas **20**, 082129 (2013).
[22]D. Winske and N. Omidi, *in Computer Space Plasma Physics: Simulations and Software*, edited by H. Matsumoto and Y. Omura (Terra, Tokyo, 1993), p. 103.
[23]R. W. Hockney and J. W. Eastwood, *Computer Simulation Using Particles* (Adam Hilger, Bristol, New York, 1989).
[24]K. S. Yee, IEEE Trans. Antennas Propag. **14**, 302 (1966).
[25]O. Buneman, "TRISTAN: The 3-D electromagnetic particle code," in *Computer Space Plasma Physics: Simulations and Software*, edited by H. Matsumoto and Y. Omura (Terra, Tokyo, 1993), p. 67.
[26]D. Winske, L. Yin, N. Omidi, H. Karimabadi, and K. Quest, "Hybrid simulation codes: Past, present and future – a tutorial," in *Space Plasma Simulation*, Lecture Notes in Physics, edited by J. Büchner, M. Scholer, and C. T. Dum (Springer, Berlin, Heidelberg, 2003), Vol. 615, p. 136.
[27]J. Müller, S. Simon, U. Motschmann, J. Schüle, K.-H. Glassmeier, and G. J. Pringle, Comput. Phys. Commun. **182**, 946 (2011).
[28]Y. C. Kim, J. M. Beall, E. J. Powers, and R. W. Miksad, Phys. Fluids (1958–1988) **23**, 258 (1980).
[29]C. Holland, G. R. Tynan, P. H. Diamond, R. A. Moyer, and M. J. Burin, Plasma Phys. Controlled Fusion **44**, A453 (2002).
[30]R. A. Moyer, G. R. Tynan, C. Holland, and M. J. Burin, Phys. Rev. Lett. **87**, 135001 (2001).
[31]T. Yamada, S.-I. Itoh, T. Maruta, N. Kasuya, Y. Nagashima, S. Shinohara, K. Terasaka, M. Yagi, S. Inagaki, Y. Kawai, A. Fujisawa, and K. Itoh, Nat. Phys. **4**, 721 (2008).